Evidence for pH-dependent multiple conformers in iron(II) heme–human serum albumin: spectroscopic and kinetic investigation of carbon monoxide binding

Yu Cao, Francesco P. Nicoletti, Giampiero De Sanctis, Alessio Bocedi, Chiara Ciaccio, Francesca Gullotta, Gabriella Fanali, Grazia R. Tundo, et al.

Volume 16 · Number 1 · January 2011

JBIC 2011

Journal of Biological Inorganic Chemistry

A Publication of the Society of Biological Inorganic Chemistry

Springer

Springer

ORIGINAL PAPER

Evidence for pH-dependent multiple conformers in iron(II) heme–human serum albumin: spectroscopic and kinetic investigation of carbon monoxide binding

Yu Cao · Francesco P. Nicoletti · Giampiero De Sanctis · Alessio Bocedi · Chiara Ciaccio ·
Francesca Gullotta · Gabriella Fanali · Grazia R. Tundo · Alessandra di Masi ·
Mauro Fasano · Giulietta Smulevich · Paolo Ascenzi · Massimo Coletta

Abstract Human serum albumin (HSA), the most prominent protein in plasma, is best known for its exceptional ligand binding capacity. HSA participates in heme scavenging by binding the macrocycle at fatty acid site 1. In turn, heme endows HSA with globin-like reactivity and spectroscopic properties. A detailed pH-dependent kinetic and spectroscopic investigation of iron(II) heme–HSA and of its carbonylated form is reported here. Iron (II) heme–HSA is a mixture of a four-coordinate intermediate-spin species (predominant at pH 5.8 and 7.0), a five-coordinate high-spin form (mainly at pH 7.0), and a six-coordinate low-spin species (predominant at pH 10.0). The acidic-to-alkaline reversible transition reflects conformational changes leading to the coordination of the heme Fe(II) atom by the His146 residue via its nitrogen atom, both in the presence and in the absence of CO. The presence of several species accounts for the complex, multiexponential kinetics observed and reflects the very slow interconversion between the different species observed both for CO association to the free iron(II) heme–HSA and for CO dissociation from CO–iron(II) heme–HSA as a function of pH.

Keywords Iron(II) heme–human serum albumin ·
Carbon monoxide · Resonance Raman · Kinetics ·
Allostery

Abbreviations

4cIS	Four-coordinate intermediate spin
5cHS	Five-coordinate high spin
6cLS	Six-coordinate low spin
FA	Fatty acid
HDL	High-density lipoproteins

Y. Cao · G. De Sanctis · C. Ciaccio · F. Gullotta ·
G. R. Tundo · M. Coletta (✉)
Department of Experimental Medicine
and Biochemical Sciences,
University of Rome "Tor Vergata",
Via Montpellier 1,
00133 Rome, Italy
e-mail: coletta@seneca.uniroma2.it

Y. Cao · A. di Masi · P. Ascenzi
Department of Biology,
University Roma Tre,
Rome, Italy

F. P. Nicoletti · G. Smulevich
Department of Chemistry "Ugo Schiff",
University of Florence,
Florence, Italy

A. Bocedi
Department of Molecular Genetics and Microbiology,
Duke University,
Durham, NC, USA

C. Ciaccio · F. Gullotta · G. R. Tundo · G. Smulevich ·
M. Coletta
Interuniversity Consortium on the Research of Chemistry
of Metals in Biological Systems, Bari, Italy

G. Fanali · M. Fasano
Department of Structural and Functional Biology,
Center of Neuroscience,
University of Insubria,
Busto Arsizio, VA, Italy

HSA   Human serum albumin
LDL   Low-density lipoproteins

Introduction

Human serum albumin (HSA), the most prominent protein in plasma (approximately 7.5×10^{-4} M HSA), is best known for its exceptional ligand binding capacity. Among others, HSA appears (1) to be an important determinant of the pharmacokinetic behavior of many drugs, (2) to account for most of the antioxidant capacity of human serum, and (3) to display enzymatic properties [1–11].

HSA is a single nonglycosylated all-α chain protein, constituted by 585 amino acids, containing three homologous domains (labeled I, II, and III). Each domain consists of two separate helical subdomains (named A, encompassing helices h1–h6, and B, encompassing helices h7–h10) connected by random coils. Terminal regions of sequential domains contribute to the formation of interdomain h10–h1 helices linking subdomain IB to subdomain IIA and subdomain IIB to subdomain IIIA, respectively (Fig. 1) [2, 3, 10–17].

The structural organization of HSA provides a variety of ligand binding sites (Fig. 1). According to Sudlow's nomenclature, bulky heterocyclic anions bind preferentially to Sudlow's site I (located in subdomain IIA), whereas Sudlow's site II (located in subdomain IIIA) is preferred by aromatic carboxylates with an extended conformation (Fig. 1) [3, 11, 18–24]. Among others, HSA is able to bind 7 equiv of long-chain fatty acids (FAs) at multiple binding sites (labeled FA1 to FA7) (Fig. 1) [11, 15, 25–28].

HSA undergoes pH- and ligand-dependent reversible conformational transition(s). Between pH 2.7 and 4.3, HSA assumes the fast-migrating form, characterized by an increase in viscosity, much lower solubility, and a significant loss of helical content. Between pH 4.3 and 8.0 and in the absence of ligands, HSA displays the neutral form, which is characterized by the typical heart-shaped structure. At pH > 8.0 and in the absence of ligands, HSA exhibits the basic form, which is characterized by a high affinity for some ligands (e.g., heme). Ligands that bind with the highest affinity to one of the conformational states may allosterically modulate the HSA transition [3, 8, 20, 22, 29–32].

The FA1 binding site has been shown to be the primary binding site of several ligands, including the heme [14, 33]. There is increasing evidence that FA1 has evolved to selectively bind iron(III) heme with high affinity ($K_d \sim 10^{-8}$ M) [14–16, 29, 33]. The tetrapyrrole ring is arranged in a D-shaped cavity delimited by the Tyr138 and Tyr161 residues, which have a π–π stacking interaction with the porphyrin and supply a donor oxygen (from
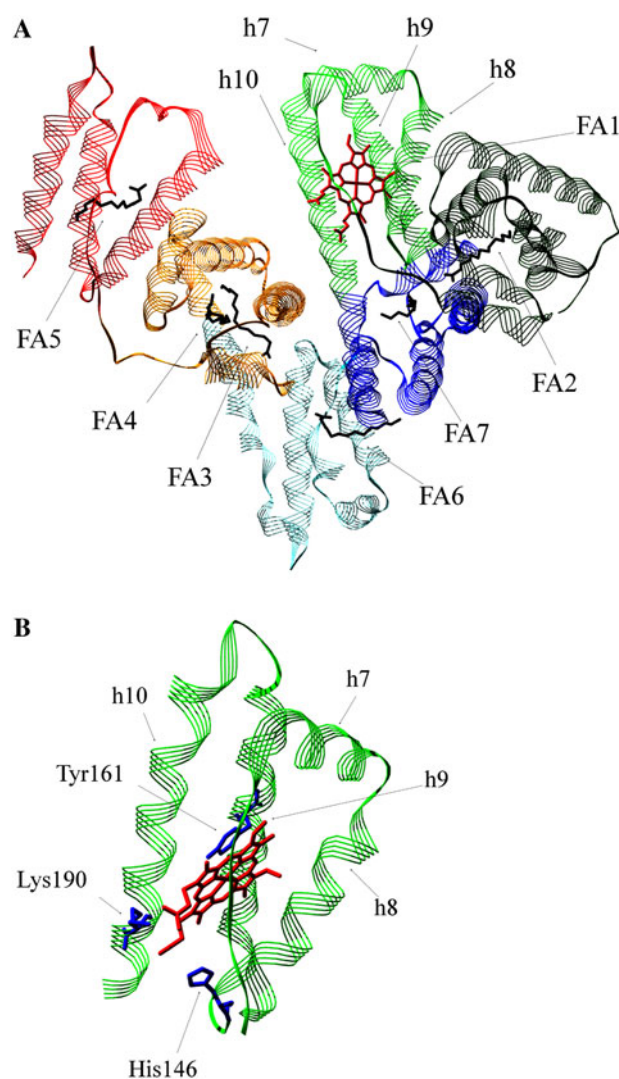
Fig. 1 **a** Human serum albumin (HSA) structure. The six subdomains of HSA are colored as follows: *dark green* subdomain IA, *light green* subdomain IB, *blue* subdomain IIA, *cyan* subdomain IIB, *orange* subdomain IIIA, *red* subdomain IIIB. The heme (*red*) binds to its primary cleft in subdomain IB. Different fatty acid binding sites (from *FA1* to *FA7*) are indicated. Helices h7–h10 are labeled. **b** Zoom of the heme binding pocket. Heme (*red*) is bound to the cleft formed by helices h7–h10. Residues His146, Tyr161, and Lys190 are shown. Atomic coordinates are taken from Protein Data Bank entry 1N5U [14]

Tyr161) for the heme Fe(III) atom. The iron(III) heme propionates protrude from the pocket, pointing toward the interface between domains I and III and are stabilized by salt bridges with His146 and Lys190. A weak coordination between the iron(III) heme and the phenolic oxygen atom of the Tyr161 residue (Fe–O_{Tyr161} distance 2.73 Å) was suggested by crystallography [14, 33] and further confirmed by resonance Raman spectroscopy [34]. Iron(III) heme is secured to HSA by the long IA–IB connecting loop that fits into the cleft opening [14–16, 29, 33, 34]. In turn, heme endows HSA with globin-like reactivity [4, 35–39] and spectroscopic properties [22, 30–32, 34, 40–43].

HSA is crucial for heme scavenging, providing protection against free heme oxidative damage, limiting the access of pathogens to heme, and contributing to iron homeostasis by recycling the heme iron. In fact, during the first seconds after the appearance of heme in plasma, more than 80% of this powerful oxidizer binds to high-density lipoproteins (HDL) and low-density lipoproteins (LDL), and only the remaining 20% binds to HSA and hemopexin. This first kinetic effect, due to the faster heme binding rate for HDL and LDL, is followed by a slower heme transfer to HSA and hemopexin, which have a higher affinity for heme. Heme binding confers on HSA globin-like spectroscopic and reactivity properties [11, 42, 44, 45]; in addition, HSA–heme has been reported to facilitate scavenging of reactive nitrogen species [46, 47]. Furthermore, since the rate of heme transfer from HDL and LDL to HSA and hemoproteins is faster than the heme-induced lipoprotein oxidation [8, 48, 49], the formation of HSA–heme represents a protective event, which prevents the formation of oxidized HDL and LDL, which are the most oxidatively intolerant plasma components. Afterwards, heme transits from HSA to hemopexin, which releases it into hepatic parenchymal cells after internalization of the hemopexin–heme complex by CD91-receptor-mediated endocytosis. Lastly, HSA–heme mutants have been reported to act as O_2 carriers, which may be useful as transfusion alternatives in clinical situations [45]. Remarkably, both heme binding to HSA and HSA–heme spectroscopic and reactivity properties are modulated competitively and allosterically, such that HSA(–heme) could be considered as a prototypical monomeric allosteric protein [11].

Here, a detailed spectroscopic and functional characterization of iron(II) heme–HSA carbonylation in the acidic, neutral, and alkaline pH regions is reported. To have a substantially unique (more than 98%) heme-bound site (i.e., FA1 site, see Fig. 1), we employed substoichiometric amounts of heme (with a heme to HSA ratio of 1:1.7). The kinetics were investigated by a rapid-mixing stopped-flow technique and were analyzed in parallel with CO rebinding data obtained after laser photolysis of CO–iron(II) heme–HSA [50]. The data obtained indicate the presence of multiple iron(II) heme–HSA and CO–iron(II) heme–HSA conformers whose relative amounts are pH-dependent. Indeed, iron(II) heme–HSA is a mixture of a four-coordinate intermediate-spin (4cIS) species which is predominant at pH 5.8 and 7.0, and which coexists with a minor five-coordinate high-spin (5cHS) form, and a six-coordinate low-spin (6cLS) species (predominant at pH 10.0). The acidic-to-alkaline reversible transition reflects conformational changes leading to the coordination of the heme Fe(II) atom by the His146 residue via its nitrogen atom, both in the presence and in the absence of CO. Accordingly, the presence of several species accounts for the complex,

multiexponential kinetics of iron(II) heme–HSA carbonylation and CO–iron(II) heme–HSA decarbonylation as a function of pH, reflecting the very slow interconversion between the different species. This investigation may also have some physiopathological significance in view of the large amount of HSA in the bloodstream and of its role as a heme scavenger during hemolytic processes, rendering the levels of heme–HSA relevant under these conditions.

Materials and methods

Materials

HSA (purity 96% or greater, essentially FA free) and hemin [iron(III) protoporphyrin IX; iron(III) heme] chloride were obtained from Sigma-Aldrich (St. Louis, MO, USA). Gaseous CO and ^{13}CO were purchased from Rivoira (Milan, Italy) and FluoroChem (Hadfield, UK), respectively. Sodium dithionite was obtained from Fluka Chemicals (Buchs, Switzerland). All other chemicals were obtained from Merck (Darmstadt, Germany). All chemicals were of analytical or reagent grade and were used without further purification.

Sample preparation

The HSA stock solution was prepared by dissolving HSA in 1.0×10^{-1} M phosphate buffer at pH 7.0 to give a final concentration of 2.0×10^{-3} M. The HSA concentration was determined spectrophotometrically at 280 nm ($\varepsilon_{280 \text{ nm}} = 38.2 \times 10^3$ M^{-1} cm^{-1}) [51]. The iron(III) heme stock solution was prepared by dissolving iron(III) heme in 1.0×10^{-1} M NaOH to give a final concentration of approximately 3×10^{-3} M. The iron(III) heme concentration was determined spectrophotometrically at 535 nm, after converting iron(III) heme to the bisimidazolate–iron(III) heme derivative by adding 1.0 M imidazole, in sodium dodecyl sulfate micelles ($\varepsilon_{535 \text{ nm}} = 14.5 \times 10^3$ M^{-1} cm^{-1}) [52]. An appropriate amount of the iron(III) heme solution was added to the HSA solution to give a final iron(III) heme to HSA ratio of 1:1.7. The iron(III) heme–HSA concentration was determined spectrophotometrically at 404 nm ($\varepsilon_{404 \text{ nm}} = 99.2$ mM^{-1} cm^{-1}). Samples at pH 5.8 and 10.0 were prepared by diluting the iron(III) heme–HSA stock solution at pH 7.0 in the appropriate 1.0×10^{-1} M phosphate or glycine buffer, respectively, and then waiting for 1 h. Iron(II) heme–HSA samples were prepared by addition of a freshly prepared sodium dithionite stock solution (1.1×10^{-1} M) to the deoxygenated iron(III) heme–HSA solution (5% v/v final concentration of sodium dithionite). CO–iron(II) heme–HSA was prepared by degassing the iron(III) heme–HSA solution by flushing it first with N_2, then

with CO or ^{13}CO and subsequently reducing the iron(III) heme–HSA by addition of a freshly prepared sodium dithionite stock solution (1.1×10^{-1} M) (5% v/v final concentration of sodium dithionite). The concentration of iron(II) heme–HSA and CO–iron(II) heme–HSA used for electronic absorption and resonance Raman spectroscopy ranged between 2.0×10^{-5} and 1.5×10^{-3} M. For kinetic experiments, 1.0×10^{-5} M iron(II) heme–HSA and CO–iron(II) heme–HSA sample solutions were used.

Spectroscopic characterization

Electronic absorption spectra of iron(III) heme–HSA, iron(II) heme–HSA, and CO–iron(II) heme–HSA were measured with a double-beam Cary 5 spectrophotometer (Varian, Palo Alto, CA, USA) using a 5-mm NMR tube or a 1-mm cuvette, and a 600 nm/min scan rate. The resonance Raman spectra of iron(II) heme–HSA were obtained using a 5-mm NMR tube and by excitation with the 413.1-nm line of a Kr$^+$ laser (Innova 300 C, Coherent, Santa Clara, CA, USA) and the 441.6-nm line of a HeCd laser (IK4121RG, Kimmon, Tokyo, Japan). Backscattered light from a slowly rotating NMR tube was collected and focused into a triple spectrometer (consisting of two Acton Research SpectraPro 2300i spectrometers and a SpectraPro 2500i spectrometer in the final stage with a 1,800 or 3,600 grooves per millimeter grating) working in the subtractive mode, equipped with a liquid-N$_2$-cooled CCD detector. The spectral resolution of the resonance Raman spectra cited in the figure captions is that calculated theoretically on the basis of the optical properties of the spectrometer. However, for the moderately broad experimental resonance Raman bands observed in the present study (approximately 10 cm^{-1}), the effective spectral resolution will, in general, be lower. To improve the signal-to-noise ratio, a number of spectra were accumulated and summed only if no spectral differences were noted. To minimize the heme Fe(II) atom oxidation under laser irradiation, samples at pH 5.8 were cooled by a gentle flow of N$_2$ gas passed through liquid N$_2$. The resonance Raman spectra were calibrated with indene, CCl$_4$, dimethyl sulfoxide, and pyridine as standards to an accuracy of ± 1 cm^{-1} for intense isolated bands. Electronic absorption spectra and resonance Raman spectra of heme–HSA derivatives were obtained at 25 °C between pH 5.8 and 10.0.

Kinetics of CO binding to iron(II) heme–HSA

The kinetics of CO dissociation from CO–iron(II) heme–HSA and of CO association to iron(II) heme–HSA were studied at 25 °C and between pH 4.8 and 10.5, employing a rapid-mixing stopped-flow apparatus (Applied Physics, Salisbury, UK) (time resolution 1 ms).

Kinetics of CO dissociation from CO–iron(II) heme–HSA

CO dissociation kinetics were studied by mixing a CO-saturated iron(II) heme–HSA solution [the final CO–iron(II) heme–HSA concentration was 5.0×10^{-6} M], in the presence of sodium dithionite (final concentration 1.1×10^{-2} M), with a degassed buffered solution containing NaNO$_2$ (final concentration 5.0×10^{-3} M) [53].

Kinetics of CO association to iron(II) heme–HSA

CO association kinetics were studied by mixing an unliganded iron(II) heme–HSA solution [the final iron(II) heme–HSA concentration was 3.0×10^{-6} M], in the presence of sodium dithionite (final concentration 1.1×10^{-2} M), with a degassed buffered solution equilibrated with CO (the final ligand concentration ranged between 1.5×10^{-5} and 5.0×10^{-4} M) [53].

Data analysis

Kinetic progress curves of CO dissociation from CO–iron(II) heme–HSA and of CO association to iron(II) heme–HSA were analyzed according to Eq. 1:

$$A_{\text{obs}} = A_0 \pm \sum_{i=1}^{i=n} \Delta A_i \cdot \exp(-^i k \cdot t), \tag{1}$$

where A_{obs} is the observed absorbance at 414 nm after a given time interval, A_0 is the absorbance at $t = 0$, n is the number of exponentials, ΔA_i is the absorbance change associated with the ith exponential, $^i k$ is the rate constant of the ith exponential (either CO association or CO dissociation rate constant), and t is the time; the sign $\pm$ is related to the possibility that during the reaction the absorbance can either increase or decrease.

The pH dependence of the observed rate constants was analyzed according to Eq. 2:

$$k_{\text{obs}} = \frac{\sum_{i=0}^{i=n} {}^i k \cdot \prod_{r=0}^{r=i} K_r \cdot [\text{H}^+]^r}{\sum_{i=0}^{i=n} \prod_{r=0}^{r=i} K_r \cdot [\text{H}^+]^r}, \tag{2}$$

where k_{obs} is the rate constant (either CO association or CO dissociation) at a given pH value, $^i k$ is the rate constant of the ith protonated species (with $^0 k$ corresponding to the rate constant of the unprotonated form at very alkaline pH values), K_r is the proton binding affinity for the rth protonated group (with $K_0 = 1$), and [H$^+$] is the proton concentration.

The population percentage is defined at each pH value by the relative amplitude (i.e., ΔA) of one exponential with respect to the total amplitude of the kinetic progress curve (expressed as the sum of all ΔA). It is expressed through Eq. 3:

$$^{i}P = \frac{\Delta A_i}{\sum_{m=1}^{m=n} \Delta A_m}, \tag{3}$$

where ^{i}P is the relative percentage of species i, m (1, 2, 3, …, n) is the degree of the species (or exponential) under consideration, n is the total number of species observed, and ΔA_i is the optical amplitude of the exponential corresponding to species i.

The pH-dependent behavior of each species i was analyzed according to Eq. 4:

$$P_{obs} = P_0 \pm \Delta P_1 \cdot \frac{K_1 \cdot [\text{H}^+]}{1 + K_1 \cdot [\text{H}^+] + K_1 \cdot K_2 \cdot [\text{H}^+]^2} \pm \Delta P_2$$
$$\cdot \frac{K_1 \cdot K_2 \cdot [\text{H}^+]^2}{1 + K_1 \cdot [\text{H}^+] + K_1 \cdot K_2 \cdot [\text{H}^+]^2}, \tag{4}$$

where P_{obs} is the observed percentage of each species i at a given pH value, P_0 is the percentage of species i in the unprotonated form (i.e., at very alkaline pH values), ΔP_1 and ΔP_2 are the percentage variations of species i upon the first and the second protonation, respectively, K_1 and K_2 are the binding affinity equilibrium constants for the first and the second protonating group, respectively (such that $pK_1 = \log K_1$ and $pK_2 = \log K_2$), and $[\text{H}^+]$ is the proton concentration.

Results

Spectroscopic properties of iron(II) heme–HSA

In agreement with previous results [34, 38], the UV–vis spectrum of iron(II) heme–HSA at pH 7.0 is characterized by a broad Soret band centered at 418 nm, with two shoulders at 405 and 424 nm, and β and α bands at 536 and 572 nm, respectively (Fig. 2a). The 413.1-nm excitation resonance Raman spectrum (Fig. 2b), in resonance with the Soret band at 418 nm, shows the presence of a predominant 4cIS Fe(II) species (v_4 at 1,370 cm^{-1}, v_3 at 1,502 cm^{-1}, v_2 at 1,580 cm^{-1}, v_{10} at 1,635 cm^{-1}) in equilibrium with a 5cHS Fe(II) species (v_4 at 1,358 cm^{-1}, v_3 at 1,472 cm^{-1}, v_2 at 1,557 cm^{-1}, v_{10} at 1,602 cm^{-1}). This latter form has been proposed to correspond to a 5cHS species containing a tyrosinate (possibly Tyr161) [14] coordinated to the iron(II) heme, whereas the formation of a 4cIS species is a consequence of the weakness of the heme Fe(II)–O$_{\text{Tyr}}$ bond [34]. A small amount of a 6cLS Fe(II) species (Soret band at 424 nm, α band at 559 nm, and v_3 at 1,492 cm^{-1}) is also observed.

When the pH is decreased from 7.0 to 5.8, the relative intensities of the resonance Raman bands change (Fig. 2b), clearly indicating that the amount of the 4cIS form increases and the amount of the 6cLS species diminishes as the Soret band sharpens at 424 nm (Fig. 2a); it is not clear if any change in the amount of the 5cHS species occurs. At pH values lower than 5.8, the iron(II) heme–HSA complex is not stable enough for spectroscopic characterization and, in agreement with previous findings [4], free heme was detected.

At pH 10.0, the 6cLS species becomes the predominant form and the 4cIS and 5cHS species remain in trace amounts. The UV–vis spectrum of the 6cLS species (Fig. 2a) resembles very closely that obtained upon complexation of iron(II) heme with 2-methylimidazole [34] as well as that of iron(II) *Herbaspirillum seropedicae* truncated hemoglobin [54]. Therefore, we assign the 6cLS form to a iron(II) heme coordinated to the oxygen atom of Tyr161 and the nitrogen atom of His146. This hypothesis agrees with our previous finding that an allosteric conformational transition, induced by ibuprofen binding, moves the His146 residue close to the heme Fe(III) atom. This residue is about 9 Å from the heme iron; therefore, significant changes in the heme cavity site can be foreseen [34]. The crystal structure of iron(III) heme–HSA in the presence of ibuprofen is not available, but a model study, made by energy minimization of the heme structure within the heme binding cleft of the HSA–ibuprofen complex [24], has revealed an appreciable tilt of α-helix h10 and a reorientation of α-helix h7 [34]. Accordingly, we suggest that at alkaline pH the formation of the His146–Fe(II)–Tyr161 6cLS species derives from a shift of α-helix h8 (as a consequence of the tilt of α-helix h10 and of the reorientation of α-helix h7); this leads to a rotation of the His146 residue toward the heme Fe(II) atom (Fig. 1).

Spectroscopic properties of CO–iron(II) heme–HSA

On the basis of the findings that a conformational change(s) occurs in iron(II) heme–HSA upon a change in pH [altering the ligand coordination state of iron(II) heme–HSA], we extended the previous study on the CO–iron(II) heme–HSA adduct at pH 7.0 [34] to different pH values in order to gain insight into the pH-dependent conformational changes occurring at the heme binding site (i.e., at FA1). In fact, heme-bound CO is a sensitive probe for investigating distal and proximal effects on ligand binding of heme proteins since back-donation from the heme Fe(II) atom $d\pi$ orbitals to the CO π^* orbitals is modulated by polar interactions between the oxygen atom of the iron(II) heme bound CO and distal polar residues, and by a *trans*-ligand effect, i.e., variations in the donor strength of the *trans* ligand. As the back-donation increases, the Fe–C bond strengthens and the CO bond weakens, thereby increasing the $v(\text{Fe–CO})$ vibrational frequencies and decreasing the $v(\text{CO})$ frequencies [55–57].
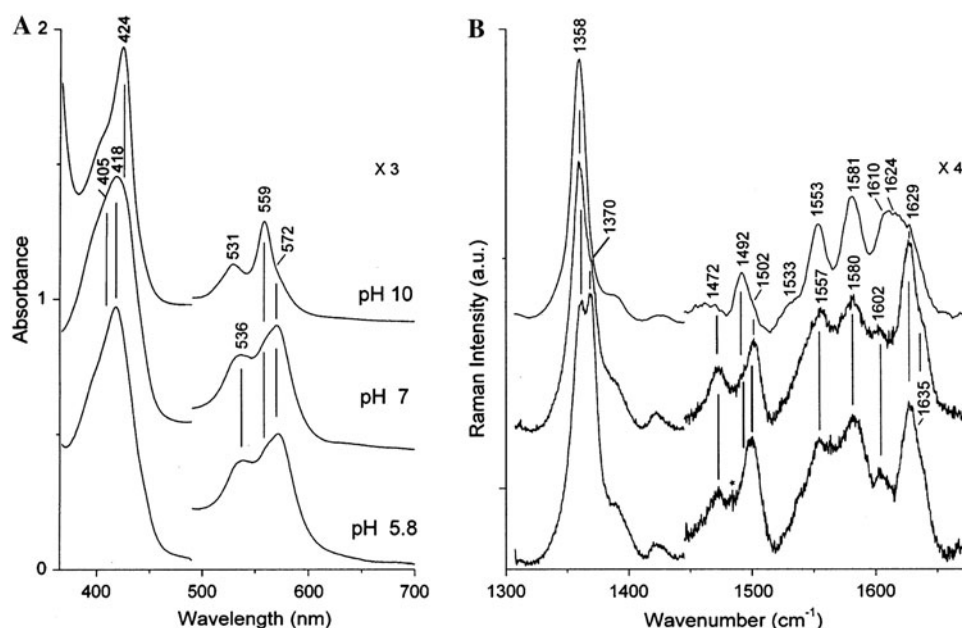
Fig. 2 Electronic absorption (**a**) and resonance Raman (**b**) spectra of iron(II) heme–HSA at pH 5.8, 7.0, and 10.0 at 25 °C. The experimental conditions were as follows: **a** 600 nm/min scan rate, **b** 413.1-nm excitation wavelength, 1.1-cm^{-1} spectral resolution (pH 7.0 and 5.8), 3.8-cm^{-1} spectral resolution (pH 10.0); at pH 5.8, 2-mW laser power at the sample, average of 30 spectra with 120-s integration time; at pH 7.0, 17-mW laser power at the sample, average of six spectra with 300-s integration time; at pH 10.0, 10-mW laser power at the sample, average of four spectra with 120-s integration time. The intensities are normalized to that of the v_4 band. The *asterisk* indicates the small amount of the iron(III) heme–HSA form due to the easy oxidation of the sample at pH 5.8. Spectra have been shifted along the ordinate axis to allow better visualization

As previously reported [34, 37], upon addition of CO to iron(II) heme–HSA at pH values between 5.8 and 7.0, the electronic absorption spectrum is characterized by a sharp Soret band centered at 416 nm and β and α bands at 536 and 569 nm, respectively (Fig. S1). The blueshift of the Soret absorption band, as compared with that of the Fe(II)–CO complexes of heme proteins having an imidazole as the fifth axial ligand ($\lambda_{max} = 420$ nm), has been interpreted as a CO–iron(II) heme adduct with a *trans* ligand weaker than His, or no ligand at all [34]. At pH 10.0, the 4-nm redshift of the Soret band (Fig. S1) strongly suggests a conformational transition which allows the weak *trans* CO–iron(II) heme ligand to be replaced by an amino acid residue coordinating the heme Fe(II) atom with a nitrogen atom. Accordingly, the resonance Raman spectra of CO–iron(II) heme–HSA at pH 7.0 and 10.0 (Fig. 3) clearly show a change in the relative intensity of the v(Fe–CO) and v(CO) stretching modes (Table 1). At pH 10.0, the strong bands at 524 cm^{-1} [v(Fe–CO)] and at 1,960 cm^{-1} [v(CO)], observed at pH 7.0 [34], decrease in intensity; concomitantly, a band at 498 cm^{-1} [v(Fe–CO)] becomes clearly evident. The corresponding v(CO) stretch could possibly be assigned to the shoulder at 1,970 cm^{-1}. It must be noted that a very weak band at 498 cm^{-1} is also present in a very low amount at pH 7.0. Accordingly, a change of the excitation wavelength from 413.1 to 441.6 nm, i.e., in resonance with the Soret band at 420 nm (Fig. S1), leads to

a substantial enhancement of the 498-cm^{-1} resonance Raman band relative to the 524-cm^{-1} band (Fig. S2).

For a large class of CO adducts of ferrous heme proteins and heme model compounds containing an imidazole as the fifth heme Fe(II) atom axial ligand, a linear correlation between the frequencies of the v(Fe–CO) and v(CO) stretching modes has been found. The correlation plots have a negative slope and depend on the extent of π back-bonding. Furthermore, since Fe–CO back-bonding is also modulated by variations in the donor strength of the *trans* axial ligand, changes in the *trans* ligand donor strength shift the correlation line and give rise to parallel lines at higher or lower positions in the correlation plot [55–57].

In the inset in Fig. 3, a plot of the v(Fe–CO) and v(CO) frequencies for CO adducts of a variety of ferrous heme proteins and heme model compounds having either a His residue as the fifth axial ligand or a weaker/absent *trans* ligand is shown [57]. The v(Fe–CO) stretching mode at 524 cm^{-1} and the v(CO) stretch at 1,960 cm^{-1} of the CO–iron(II) heme–HSA complex at pH 7.0 are located above the His line of the v(Fe–CO)/v(CO) back-bonding correlation, since the proximal ligand is either weak [55] or absent [56]. This result is consistent with the presence of a Tyr residue as the axial ligand. However, the correlation plot cannot effectively separate a five-coordinate CO–iron(II) heme system from a six-coordinate species with a weak proximal ligand, such as water or Tyr [57, 58]. The v(Fe–CO)/v(CO)
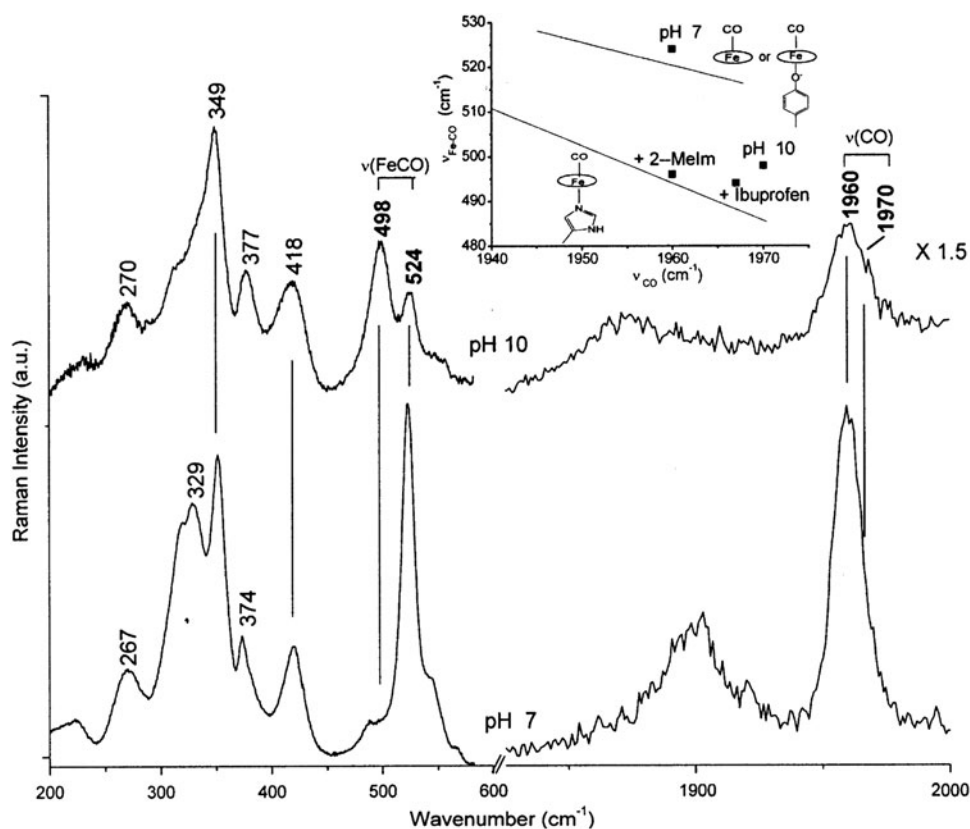
Fig. 3 Resonance Raman spectra of CO–iron(II) heme–HSA at pH 7.0 and 10.0, at 25 °C. The experimental conditions were as follows: 413.1-nm excitation wavelength; 1- and 3.3-cm^{-1} spectral resolution for the low-frequency and high-frequency regions, respectively; at pH 7.0, 15-mW laser power at the sample, average of 32 spectra with 140-s integration time (low-frequency region), average of three spectra with 600-s integration time (high-frequency region); at pH 10.0, 2-mW laser power at the sample, average of six spectra with 1,500-s integration time (low-frequency region), average of eight spectra with 600-s integration time (high-frequency region). The intensities are normalized to that of the v_4 band (not shown). Spectra have been shifted along the ordinate axis to allow better visualization. The *inset* shows the correlation plot of the v(Fe–CO) versus v(CO) frequencies observed in the CO complexes of iron(II) heme–HSA under various experimental conditions. The *lower line* indicates the back-bonding correlation line for six-coordinate CO–heme proteins with imidazole as the sixth ligand [57]. The *upper line* represents five-coordinate, with no *trans* internal axial ligand, or six-coordinate iron(II) carbonylated heme proteins with weak *trans* internal axial ligands. Data and references are given in Table 1. The respective *trans* ligands are shown. *2–MeIm*: 2-methylimidazole

stretch values of the alkaline form at pH 10.0 fall on the His v(Fe–CO)/v(CO) back-bonding correlation line (Fig. 3), closer to the values of the iron(II) heme–HSA complex in the presence of 2-methylimidazole or ibuprofen, in which the *trans* axial ligand is an imidazole or His, respectively [34]. These data confirm that at alkaline pH a major conformational change(s) occurs in the heme pocket of CO–iron(II) heme–HSA, allowing the His146 residue to coordinate the heme Fe(II) atom via its nitrogen atom, both in the presence and in the absence of CO.

Kinetics of CO binding to iron(II) heme–HSA

Kinetics of CO dissociation from CO–iron(II) heme–HSA

Figure S3 shows the time course of CO dissociation from CO–iron(II) heme–HSA upon replacement of CO with NO at two widely different pH values, namely, pH 4.8 (Fig. S3a) and pH 10.0 (Fig. S3b), followed by observation of the absorbance changes at 414 nm. At pH ≤ 7.0 this reaction can be described by Eq. 1 with three exponentials (i.e., $n = 3$, see Fig. S3a), whereas at alkaline pH only two exponentials are required (i.e., $n = 2$, see Fig. S3b). This indicates that two or three CO–iron(II) heme–HSA species are present at the respective pH values, and they interchange very slowly. The pH dependence of the CO dissociation rate constants, corresponding to the various exponentials, is reported in Fig. 4a. It displays a proton-linked behavior for the two faster exponentials, characterized by the two pK_a values reported in Table 2. On the other hand, the complex behavior observed for the relative percentage of absorption amplitudes of different exponentials (see Fig. 4b) clearly indicates that the two main exponentials refer to two pH-dependent structural

Table 1 Vibrational frequencies (cm^{-1}) of the Fe(II)–CO stretching modes in the CO adducts of selected iron porphyrins and heme proteins

Protein	v(Fe–CO)	v(CO)	Axial ligation	Reference
6c CO complexes with a weak *trans* ligand or 5c complexes with no ligand				
Iron(II) heme–HSA + ibuprofen	525 (519)	1,962 (1,924)	CO–Fe	[34]
Iron(II) heme–HSA + 2-MeIm	524 (520)	1,960 (1,912)	CO–Fe–O_{Tyr}	[34]
Iron(II) heme–HSA (pH 7.0)	524 (520)	1,960 (1,912)	CO–Fe–O_{Tyr}	[34]
HasA$_{SM}$	532 (523)	1,954 (1,905)	CO–Fe–O_{Tyr}	[63]
Human HO-1 (H25Y)	529 (524)	1,962 (1,917)	CO–Fe–OH_2	[64]
Iron(II) heme–CO in PBS (pH 6.9)	525	1,962	CO–Fe	[34]
Sperm whale Mb (pH 2.6)	526		CO–Fe–OH_2	[65]
6c CO complexes with imidazole *trans* ligand and apolar distal environment				
Iron(II) heme–HSA (pH 10.0)	498 (494)	1,970 (1,927)	CO–Fe–N_{His}	This work
Iron(II) heme–HSA + ibuprofen	494 (488)	1,967 (1,924)		[34]
Iron(II) heme–HSA + 2-MeIm	496 (492)	1,960 (1,912)	CO–Fe–N_{His}	[34]
Fe(PPDME)(Im)	495	1,960	CO–Fe–N_{His}	[66]
Sperm whale Mb				
pH 4.1	488	1,967	CO–Fe–N_{His}	[65]
pH 2.6	491		CO–Fe–N_{His}	[67]

The frequencies obtained with ^{13}CO are given in parentheses

6c six coordinate, *5c* five coordinate, *HSA* human serum albumin, *2-MeIm* 2-methylimidazole, *HasA$_{SM}$* hemophore HasA from *Serratia marcenscens*, *HO-1* heme oxygenase 1, *PBS* phosphate-buffered saline, *Mb* myoglobin, *PPDME* protoporphyrin IX dimethyl ester, *Im* imidazole

arrangements of CO–iron(II) heme–HSA. The resulting pK_a values are reported in Table 2. The third exponential, which is always less than 10% of the total amplitude, is characterized by a very slow pH-independent rate (see Fig. 4a) that disappears at pH ≥ 7.0. This suggests that it possibly corresponds to CO dissociation from aggregated free heme (also detected by the spectroscopic analysis, see earlier).

Kinetics of CO association to iron(II) heme–HSA

Figure S4 shows the time course of CO binding to iron(II) heme–HSA at two widely different pH values, namely, pH 4.8 (Fig. S4a) and pH 10.0 (Fig. S4b), followed by the observation of absorbance changes at 414 nm. At both pH values, CO binding to iron(II) heme–HSA is characterized by a multiexponential behavior, suggesting the existence of several structural arrangements of the heme pocket that likely interchange at a rate much slower than CO binding. This latter feature is supported by the experimental evidence that a pH jump of iron(II) heme–HSA from pH 7.0 to either pH 5.2 or pH 9.1 displays a very slow rate (see Fig. S5) for the pH-linked conformational change(s), indicating that this process is characterized by a rate $j < 10^{-3}$ s^{-1}. Therefore, the CO binding kinetic progress curve represents a "snapshot" of the different CO-binding iron(II) heme–HSA species present in the reaction mixture. As a consequence, the amplitude of the exponentials describing the time courses reflects the relative percentage of iron(II)

heme–HSA species, such that the percentage of each species i (i.e., P_i) at a given pH value and CO concentration can be quantified according to Eq. 3.

Figure S4 shows the markedly different kinetic pattern of iron(II) heme–HSA carbonylation at pH 4.8 and 10.0. At pH 4.8 (Fig. S4a) we observe only a small percentage of the fast CO-binding iron(II) heme–HSA species, followed by a much larger amount of a slow reacting form(s). Conversely, at pH 10.0 (Fig. S4b), the amount of the iron(II) heme–HSA species which reacts fast with CO is much greater than the amount of the slow reacting form(s). In particular, according to Eq. 1 the analysis of the CO binding kinetics at 414 nm indicates that at pH ≤ 7.0 (at least) four exponentials (i.e., $n = 4$) are required to fit the progress curves, whereas at pH ≥ 7.0, three exponentials (i.e., $n = 3$) may be sufficient.

The analysis of individual kinetic progress curves at various CO concentrations and pH values allowed us to characterize the CO dependence and the proton linkage of all CO binding rates. This first step of data analysis is reported in Fig. 5 for three representative pH values, namely, pH 4.8 (Fig. 5a), pH 7.0, (Fig. 5b), and pH 10.0 (Fig. 5c). The rate of the first exponential is always dependent on the CO concentration (see Fig. 5), indicating that it refers to CO binding to a species where either the heme Fe(II) atom is five coordinate or the endogenous coordinating ligand dissociates at a rate much faster than the pseudo-first-order rate of CO binding. Therefore, this process can be analyzed by employing Eq. 5 [53]:
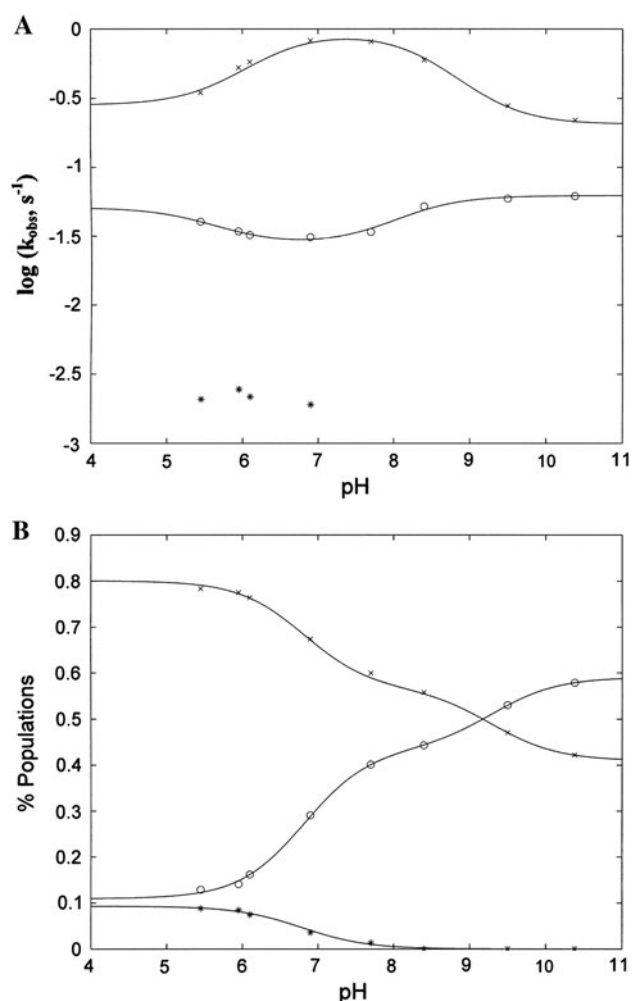
Fig. 4 pH dependence of CO dissociation rates from CO–iron(II) heme–HSA, at 25.0 °C. (**a**) pH dependence of the CO dissociation rate constants for species 1 (*open circles*), 2 (*crosses*), and 3 (*asterisks*). The *lines* were obtained by the nonlinear least-squares fitting of data, according to Eq. 2; values of pK_a are reported in Table 2. (**b**) pH dependence of the percentage of CO–iron(II) heme–HSA populations as derived from the percentage of different exponentials. The *lines* were obtained by the nonlinear least-squares fitting of data, according to Eq. 4; values of pK_a are reported in Table 2. The attribution of rate constants was based on the corresponding percentage of populations

$$k_{obs} = k_{on} \cdot [CO] + k_{off}, \tag{5}$$

where k_{obs} is the observed rate constant at a given CO concentration, k_{on} is the second-order CO association rate constant, and k_{off} is the first-order CO dissociation rate constant. The continuous lines in Fig. 5 refer to the non-linear least-squares fitting of data according to Eq. 5 for iron(II) heme–HSA carbonylation at pH 4.8 (Fig. 5a), pH 7.0 (Fig. 5b), and pH 10.0 (Fig. 5c). We conducted the analysis by imposing one of the k_{off} values obtained from direct measurements of CO dissociation; the best fit (reported in Fig. 5) was obtained by employing greater

Table 2 Values of pK_1 and pK_2 for the pH dependence of CO–iron(II) heme–HSA species (calculated according to Eq. 4) and of the kinetics of CO dissociation from CO–iron(II) heme–HSA (i.e., k_{obs} obtained by NO replacement experiments and calculated according to Eq. 2)

	pK_1	pK_2
CO–iron(II) heme–HSA species (see Fig. 4b)		
1	8.9 ± 0.2	6.6 ± 0.2
2	8.9 ± 0.2	6.6 ± 0.2
3	6.8 ± 0.2	
Rate constants for CO dissociation from CO–iron(II) heme–HSA species (see Fig. 4a)		
1	8.5 ± 0.2	6.3 ± 0.2
2	8.2 ± 0.2	5.5 ± 0.2

valuess (see Fig. 4a) obtained from the direct measurement for k_{off} at the corresponding pH value.

The second exponential displays a peculiar behavior, since its value depends on CO at low ligand concentration and levels off at high CO concentrations, indicating the existence of a rate-limiting step (see Fig. 5). This feature suggests that this CO binding process concerns a form characterized by an hexacoordinating ligand which must be displaced to permit CO binding to iron(II) heme–HSA, according to Scheme 1 [59]:

$$L-Fe(II)\text{-heme}-HSA \underset{k_{+L}}{\overset{k_{-L}}{\rightleftarrows}} Fe(II)\text{-heme}-HSA + L + CO \underset{k_{off}}{\overset{k_{on}}{\rightleftarrows}} CO-Fe(II)\text{-heme}-HSA$$

Scheme 1 Reaction scheme for the process characterized by a rate-limiting step

where L–Fe(II)-heme–HSA is the 6cLS species, Fe(II)-heme–HSA is the 5cHS species, CO–Fe(II)-heme–HSA is the CO-bound species, k_{-L} is the rate constant for the dissociation of the six-coordinate internal ligand, k_{+L} is the rate for the association of the hexacoordinating internal ligand, which competes with the association rate constant for CO binding (i.e., k_{on}), and k_{off} is the CO dissociation rate constant. According to Scheme 1, the observed rate constant k_{obs} corresponds to Eq. 6a:

$$k_{obs} = \frac{k_{-L} \cdot k_{on} \cdot [CO] + k_{off} \cdot k_{+L}}{k_{off} \cdot [CO] + k_{+L}}. \tag{6a}$$

Whenever $k_{on}[CO] \ll k_{+L}$, Eq. 6a reduces to Eq. 6b:

$$k_{obs} = \frac{k_{-L} \cdot k_{on} \cdot [CO]}{k_{+L}} + k_{off}. \tag{6b}$$

Whenever $k_{on}[CO] \gg k_{+L}$, Eq. 6a reduces to Eq. 6c:

$$k_{obs} = k_{-L} + \frac{k_{off} \cdot k_{+L}}{k_{on} \cdot [CO]}, \tag{6c}$$

which is essentially independent of CO concentration. It is important to underline that only k_{-L} and k_{off} are defined unequivocally by the application of Eqs. 6a, 6b, and 6c.

Fig. 5 CO concentration dependence of the observed carbonylation ▶ rate constants of iron(II) heme–HSA at pH 4.8 (**a**), 7.0 (**b**), and 10.0 (**c**), at 25.0 °C. The *continuous lines* were obtained by the nonlinear least-squares fitting of data to species 1 according to Eq. 5 [giving k_{on} of 6.1($\pm$0.8) $\times$ 10^6 M^{-1} s^{-1} at pH 4.8, 4.2($\pm$0.6) $\times$ 10^6 M^{-1} s^{-1} at pH 7.0, and 1.3($\pm$0.3) $\times$ 10^7 M^{-1} s^{-1} at pH 10.0]. The *dashed lines* were obtained by the nonlinear least-squares fitting of data to species 2 according to Eq. 6a. The rate constants referring to species 3 and 4 are CO-independent

These equations also allowed the parameter k_{on}/k_{+L} to be determined, representing the binding competition between CO and the hexacoordinating internal ligand for the heme Fe(II) atom [59].

The CO dependence of the second exponential suggests that it refers to an iron(II) heme–HSA species where the hexacoordinating internal ligand dissociates and reassociates fast enough to show a CO dependence of the carbonylation rate at low CO concentrations, but it becomes CO-independent at high CO concentrations (see Fig. 5). This feature suggests that for this species $k_{on}[CO] \cong k_{+L}$, such that at lower CO concentrations $k_{on}[CO] < k_{+L}$ (i.e., the system follows the behavior indicated by Eq. 6b), whereas at high CO concentrations $k_{on}[CO] > k_{+L}$ (i.e., the system is described by Eq. 6c). The dashed lines in Fig. 5 correspond to the nonlinear least-squares fitting of data for the second exponential according to Eqs. 6a, 6b, and 6c. In this case the best fit (reported in Fig. 5) was obtained by employing the smaller values of k_{off} obtained from the direct measurement of this parameter at the corresponding pH value (see Fig. 4a).

The rate(s) of the third and fourth (when present) exponential(s) is (are) always independent of the CO concentration (see Fig. 5). Also in these cases Scheme 1 can be applied; however, the CO independence of the rate constants over the whole concentration range investigated clearly indicates that these processes refer instead to hexacoordinating species which dissociate and reassociate with a much smaller rate constant, so $k_{on}[CO]$ is always much greater than both k_{+L} and k_{-L}.

Additional information can be obtained from the analysis of the CO dependence of the optical absorption amplitudes of CO–iron(II) heme–HSA species, since they should refer to the CO binding equilibrium between different species. Obviously, in the case of the simple binding process, as for the first exponential (see Eq. 5), the CO dependence is related to the intrinsic CO affinity equilibrium constant K_{CO} (which is equal to $\frac{k_{on} \times [CO]}{k_{off}}$). On the other hand, for the other exponentials, where Scheme 1 must be applied, the CO dependence refers instead to the observed CO affinity equilibrium constant K_{obs} (which is equal to $\frac{k_{-L} \cdot k_{on} \times [CO]}{k_{+L} \cdot k_{off}} = \frac{K_{CO}}{K_L}$), which represents the ratio between the intrinsic CO affinity equilibrium constant K_{CO} and the affinity equilibrium constant for the hexacoordinating internal ligand K_L (which is equal to $\frac{k_{+L}}{k_{-L}}$).
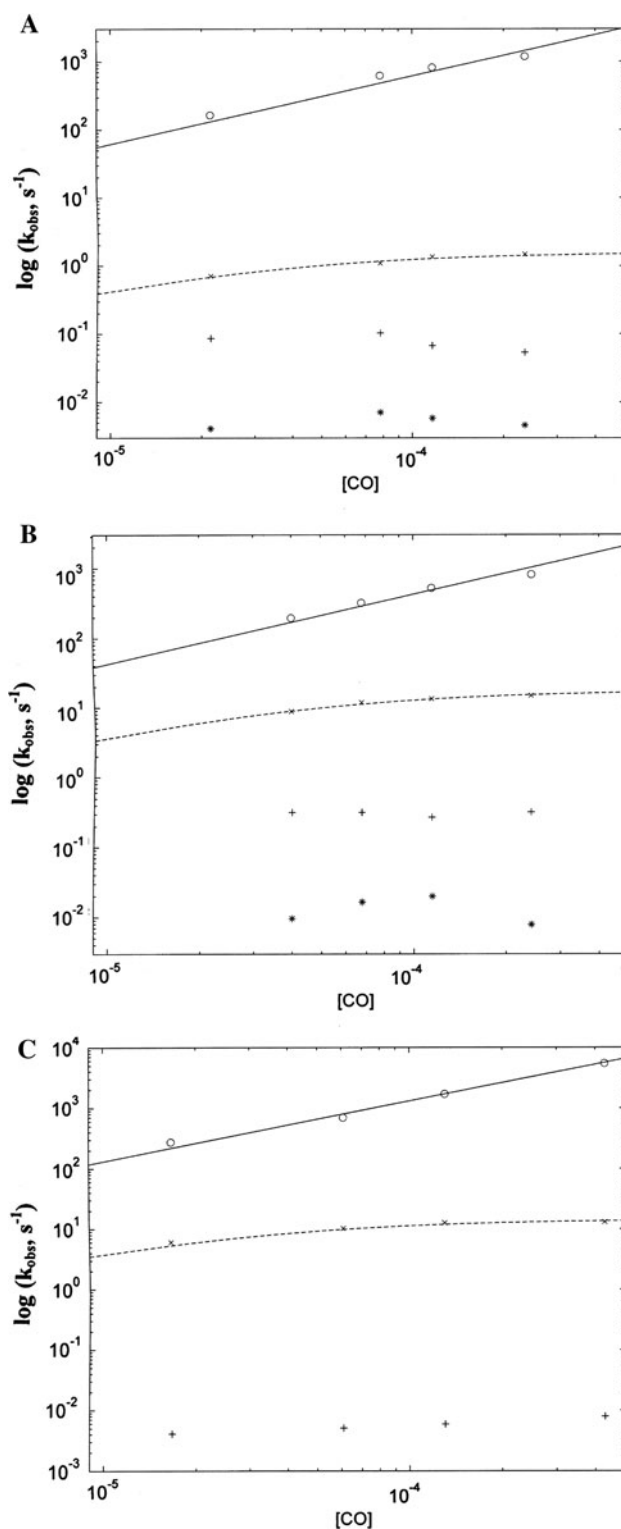

Figure S6 displays the CO dependence of the optical absorption amplitudes of various species at three indicative pH values, namely, pH 4.8 (Fig. S6a), pH 7.0 (Fig. S6b), and pH 10.0 (Fig. S6c). It is immediately evident that the values of the amplitudes of the first exponential are

Fig. 6 pH dependence of unligated iron(II) heme–HSA and CO–iron(II) heme–HSA populations. (**a**) pH dependence of the percentage of unligated iron(II) heme–HSA as derived from the percentage of different exponentials. The *lines* were obtained by the nonlinear least-squares fitting of data, according to Eq. 4; the pK_a values are reported in Table 3. The assignment of species 1 to 4 is given in the text. (**b**) pH dependence of the CO association rate constants for species 1. The *line* was obtained by the nonlinear least-squares fitting of data, according to Eq. 2; the pK_a values are reported in Table 3. (**c**) pH dependence of the rate-limiting-step kinetic constant k_{-L} (see Eq. 6c). The *line* was obtained by the nonlinear least-squares fitting of data, according to Eq. 2; the pK_a values are reported in Table 3

CO-independent at all the pH values investigated over the CO concentration range between 1.5×10^{-5} and 5.0×10^{-4} M, indicating that CO affinity is high enough to completely saturate all the five-coordinate heme species even at the lowest CO concentration. The same holds for the intermediate species and only the slowest CO binding forms (corresponding to the fourth exponential at pH ≤ 7.0 and to the third exponential at pH ≥ 7.0) are CO-concentration-dependent (see Fig. S6). The requirement of higher CO concentrations for the formation of the CO–iron(II) heme–HSA adduct indeed suggests a fairly high affinity for the hexacoordinating endogenous ligand (thus efficiently competing with CO). This feature, which possibly indicates the occurrence of different endogenous hexacoordinating ligands, was analyzed according to Eq. S1.

In this way, we obtained the value of ΔA_{tot} for the species that displays a CO dependence of the optical absorption amplitudes (for the CO-independent species the experimental values already correspond to their respective ΔA_{tot}). Therefore, applying Eq. 3 (where each $A_i = \Delta A_{tot}$ for a given form i), we calculated the pH dependence of the species distribution (Fig. 6a). The inspection of Fig. 6a allowed us to highlight that (1) the population percentage characterized by the first exponential (i.e., 5cHS) increases markedly from pH 4.8 to pH 7.0, then decreases somewhat going from pH 7.0 to pH 10.0; (2) the percentage of the species characterized by the second exponential (about 10% of the total population) seems to remain fairly constant over the whole pH range investigated; (3) the percentage of the species characterized by the third exponential decreases upon raising the pH from 4.8 to 7.0, and eventually becomes too small to be detected at pH > 7.0; (4) the percentage of the slowest CO binding form (corresponding to the fourth exponential at pH ≤ 7.0 and to the third exponential at pH >7.0) decreases markedly on increasing the pH from 4.8 to pH 7.0 (in a fashion inversely mirroring the behavior of the 5cHS species), then slightly increases between pH 7.0 and pH 10.0. The pH-dependent behavior of each species, i, was analyzed according to Eq. 4.
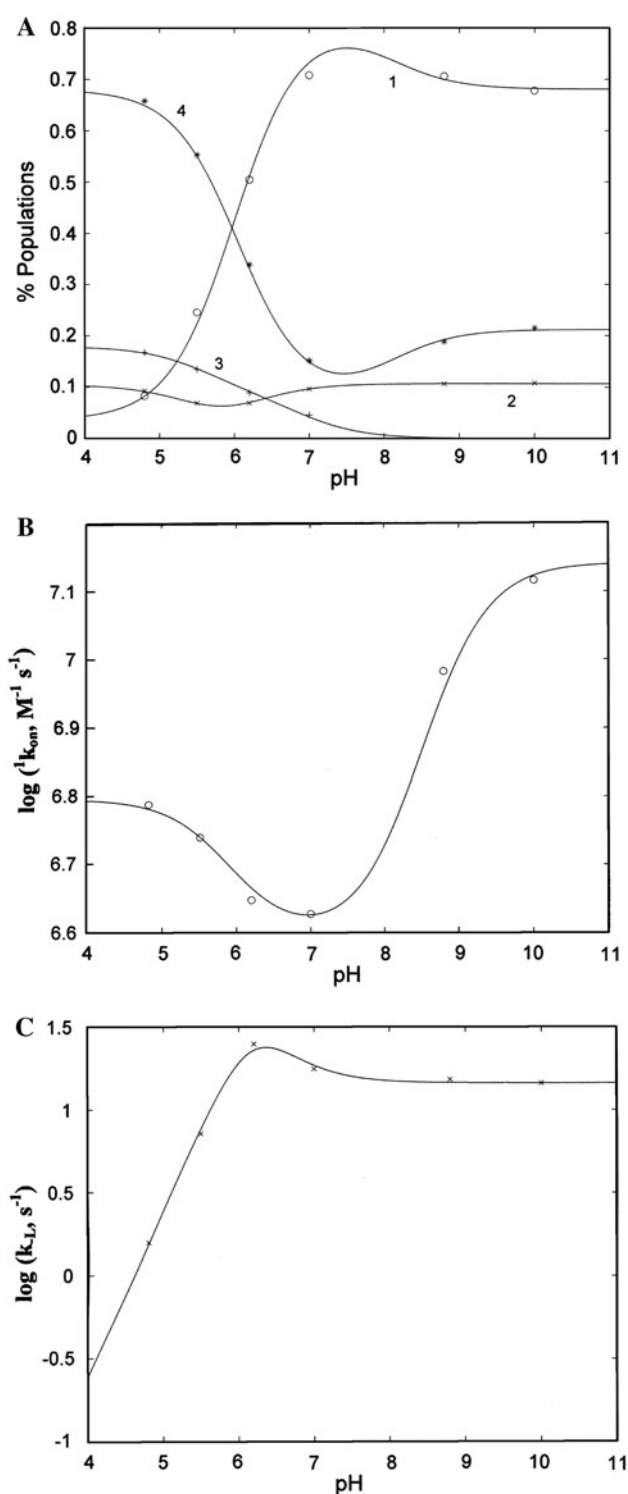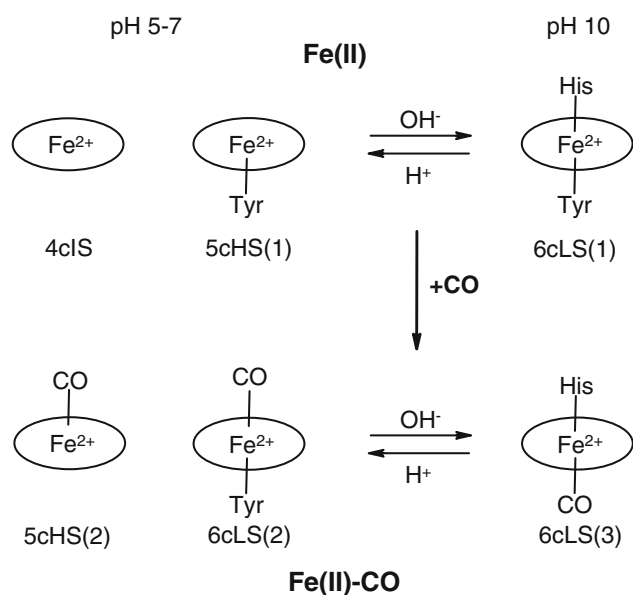

Figure 6b and c shows the pH dependence of the rate constants for CO binding to iron(II) heme–HSA; the data were analyzed according to Eq. 2. In particular, for the first exponential we indicate the pH dependence of the bimolecular rate constant for CO binding to the 5cHS species (see Fig. 6b), whereas for the second exponential we

Fig. 7 The heme iron coordination of the iron(II) heme–HSA (*top*) and CO–iron(II) heme–HSA (*bottom*) species. *Bottom* the (Fe^{2+}–CO) and (CO–Fe^{2+}–Tyr) species cannot be distinguished by resonance Raman spectroscopy. *4cIS* four-coordinate intermediate spin, *5cHS* five-coordinate high spin, *6cLS* six-coordinate low spin

Table 3 Values of pK_1 and pK_2 for the pH-dependence of iron(II) heme–HSA species (as calculated according to Eq. 4), of the kinetics of CO binding to five-coordinate high-spin (*5cHS*) iron(II) heme–HSA (i.e., k_{on}, as calculated according to Eq. 2), and of the kinetics of dissociation of the weakly bound endogenous ligand from species 2 (i.e., k_{-L}, as calculated from Eq. 2)

	pK_1	pK_2
Iron(II) heme–HSA species (see Fig. 6a)		
1	8.1 ± 0.2	6.0 ± 0.2
2	6.2 ± 0.2	5.5 ± 0.2
3	6.9 ± 0.2	5.6 ± 0.2
4	8.1 ± 0.2	6.1 ± 0.2
Kinetics of CO binding to 5cHS iron(II) heme–HSA species (see Fig. 6b)		
k_{on} (M^{-1} s^{-1})	8.8 ± 0.2	5.8 ± 0.2
Kinetics of dissociation of the weakly bound endogenous ligand from species 2 of iron(II) heme–HSA (see Fig. 6c)		
k_{-L} (s^{-1})	5.5 ± 0.2	6.8 ± 0.2

indicate the pH dependence of the rate-limiting values corresponding to k_{-L} (see above) (see Fig. 6c). All the pK_a values are reported in Table 2.

Discussion

In iron(II) heme–HSA the presence of many pH-dependent differently coordinated species (see Figs 2, 3) represents a complex scenario. In fact, the pH-dependent kinetics for CO dissociation from the CO–iron(II) heme–HSA complex and the CO binding to iron(II) heme–HSA appears quite complex, displaying several exponentials, whose percentage contribution to the total optical density change varies with pH (see Figs 4b, 6a). This feature, which reflects the very slow interconversion rates between the different species (see Fig. S5), mirrors the exchange of the axial coordination, which takes place at different pH values, as illustrated in Fig. 7.

The unliganded and the CO–iron(II) heme–HSA forms show a different pH-dependent transition between different coordination geometries, as demonstrated by the comparison between Figs. 4b and 6a and from the different pK_a values (see Tables 2, 3). Therefore, upon CO binding at different pH values, the different axial coordination likely contributes to the kinetic behavior observed. Thus, we cannot rule out that one of the kinetic patterns corresponding to the slowest CO-independent exponentials indeed reflects a change in the coordinating residue rather than CO binding.

Focusing on the CO-bound forms, the increase in pH brings about the progressive decrease of the fastest CO-dissociating form and the appearance of a slower transition characterized by two pK_a values (6.6 ± 0.2 and 8.9 ± 0.2) (see Fig. 4b; Table 2). These two pK_a values might correspond to (1) a transition (characterized by p$K_a = 6.6 \pm 0.2$) between a CO-bound five-coordinate form [without an internal *trans* axial ligand, indicated as 5cHS(2) in Fig. 7] and a CO-bound six-coordinate form [i.e., the 6cLS(2) form in Fig. 7], where the *trans* axial ligand is Tyr161 (this transition is silent in resonance Raman spectroscopy); and (2) a transition (characterized by p$K_a = 8.9 \pm 0.2$) between the 6cLS(2) species and another CO-bound six-coordinate form where the *trans* axial ligand is His146 [6cLS(3) species, Fig. 7]. The first pK_a value could be attributed to the deprotonation of the Tyr161 phenolic group that is strongly polarized by the proximity of the iron atom, whereas the second constant is associated with the neutral-to-basic conformational transition [34]. In this case, a dramatic reorientation of the h8 helix could induce the His146 side chain to protrude into the heme cavity *trans* to Tyr161. This reorientation leads to two different 6cLS species, namely, (1) the 6cLS(3) species in the CO-bound form where His146 coordinates Fe(II) axially and CO replaces Tyr161, and (2) the 6cLS(1) form (Fig. 7) in the iron(II) heme–HSA complex where both His146 and Tyr161 are axially coordinated to Fe(II). Therefore, if the second transition corresponds to the substitution of Tyr161 by His146 as a *trans* axial coordinating residue, the corresponding pK_a value (which cannot be attributed to the protonation/deprotonation of a His) must refer to the protonation of another residue(s) involved in the modulation of iron(II) heme coordination and in the neutral-to-basic transition (e.g., Lys190 and/or Arg114). In this

respect, it is interesting to underline that the substitution of Lys190 by Arg eliminates the heterogeneity of CO rebinding after photolysis to iron(II) heme–HSA [39], clearly indicating that Lys190 plays a major role in the conformation of the heme inside the FA1 site through its interaction with heme propionates. A third exponential is observed at pH ≤ 8.0 (see Fig. 4b) and is likely related to the presence of aggregated free CO-bound iron(II) heme, whose dissociation is very slow and pH-independent (see Fig. 4a).

In the case of the CO reaction with iron(II) heme–HSA, the predominance at low pH values of a very slow CO-independent binding process (Fig. 6a) indicates that either (1) the CO access to the heme pocket of the 4cIS species is very difficult, possibly impaired by a high energy barrier which can be overcome at a very slow rate, or (2) bimolecular CO binding to the 4cIS species (which is very fast, see Fig. 6b) initially leads to a five-coordinate CO-bound species [i.e., 5cHS(2) species in Fig. 7], followed by a very slow process (likely characterized by a large conformational change) involving the binding of an endogenous axial ligand *trans* to the CO in the 5cHS(2) form. The final form is, therefore, a 6cLS species, whose axial ligand is likely a Tyr residue [i.e., the 6cLS(2) species in Fig. 7]. These two species cannot be distinguished by resonance Raman spectroscopy.

As the pH is raised above 6.0, the species characterized by a bimolecular CO-dependent binding process becomes predominant. This form likely corresponds to the 5cHS(1) species (Fig. 7), where Tyr161 is the iron(II) heme axial ligand, as suggested by resonance Raman spectroscopy (see Fig. 2) and the relatively high pK_a values of the transitions (i.e., pK_a = 6.0 ± 0.2 for process 1 and pK_a = 6.1 ± 0.2 for process 4; see Fig. 6a, Table 3). In other words, this process should mirror the progressive predominance of species 5cHS(1) (Fig. 7), which simply reacts with CO, giving rise to the 6cLS(2) form (Fig. 7) without forming an intermediate. The fast bimolecular rate constant suggests the presence of a weak proximal bond in the 5cHS(1) species, compatible with the Fe(II)–O$_{Tyr161}$ bond (Fig. 7). This bimolecular rate constant is somewhat smaller than that at pH < 5.5 (see Fig. 6b), which corresponds to the reaction of CO with the 4cIS form to give the 5cHS(2) species (see Fig. 7). It is important to underline that CO binding at pH 7.0 to site-directed mutants of iron(II) heme–HSA, where Tyr161 had been substituted by either Leu or Phe [45] displays only small differences for the bimolecular rate constant of species 1 with respect to our wild type [i.e., $^1k_{on}$ = 4.2(±0.6) × 10^6 M^{-1} s^{-1} for the wild type, whereas $^1k_{on}$ = 2.0(±0.3) × 10^6 M^{-1} s^{-1} for the double mutant I142H/Y161L and $^1k_{on}$ = 6.8(±0.8) × 10^6 M^{-1} s^{-1} for the double mutant I142H/Y161F. Although some caution is required for comparison with these double mutants, since the presence of His142 might lead to an alternative

axial coordination of the heme with His142, this result seems to indicate that the removal of Tyr161 does not bring about any dramatic alteration of the bimolecular CO binding process.

The behavior of species 2 (Fig. 6a), which amounts to about 10% of the total iron(II) heme–HSA molecules, is characterized by a CO-dependent rate constant at low CO concentrations, which becomes independent of CO at higher ligand concentrations. The occurrence of a rate-limiting step suggests that CO binding displaces an endogenous ligand that is coordinated in the unliganded form, but this ligand dissociates at a rate similar to that of the pseudo-first-order CO binding rate; thus, the observation of the rate-limiting step depends on the CO concentration. The rate-limiting constant shows a slight increase as the pH is lowered from 10.0 to 6.0, but a marked decrease as the pH is lowered further (Fig. 6c). The resulting pK_a values (see Table 3 for CO binding to species 2) indicate that the rate-limiting constant is somewhat increased owing to the protonation of a group characterized by pK_a = 5.5 ± 0.2, but the effect is overwhelmed by a remarkable decrease due to the protonation of a group with pK_a = 6.8 ± 0.2. Therefore, species 2 may correspond to the 6cLS(1) form (Fig. 7), the axial ligands being His146 and Tyr161, and the rate-limiting step for CO binding to iron(II) heme–HSA at alkaline pH should correspond to the dissociation of Tyr161. This being the case, the relatively fast dissociation rate of this endogenous axial ligand at alkaline pH suggests that this Tyr residue (i.e., Tyr161) is a weakly bound axial ligand. The rate-limiting constant then slightly increases at lower pH (Fig. 6c) owing to the easier protonation of Tyr161 (possibly characterized by pK_a = 5.5 ± 0.2); at pH ≤ 6.5 a different rate-limiting step for CO binding becomes predominant, resulting in a much slower rate for the displacement of the internal ligand.

Finally, the two very small CO-independent rate constants are much less interesting. Species 3 (Fig. 6a) likely corresponds to free iron(II) heme (detected by resonance Raman spectroscopy). It binds CO very slowly and its CO-independent rate constant is limited by the dissociation of the stacked hemes. The other slow process (species 4 in Fig. 6a), whose population depends on pH in a fashion inversely mirroring that of species 1, is probably due to a slow process involving the substitution of the axial coordinating ligand. Upon CO binding, species 6cLS(2) converts to the 6cLS(3) form (see above). Therefore, as in unliganded iron(II) heme–HSA, an increase of pH brings about an increase of the population of the 5cHS(1) species at the expense of the 4cIS state. Similarly, following CO binding, a change from the 6cLS(2) to the 6cLS(3) species is observed (see Fig. 7).

In conclusion, the kinetics of CO dissociation from CO–iron(II) heme–HSA and CO association to iron(II)

heme–HSA clearly reveal a complex network of ligand-linked interactions between the heme and the neighboring residues of the FA1 site. Moreover, many residues must be called into play to regulate the access and exit pathways of diatomic ligands (such as CO) to this site and to participate in the stabilization of the axial coordination of the heme and, thus, of its reactivity with the ligand(s). In addition, the growing importance of the diatomic ligand CO as a gas transducer involved in the signaling related to reactive oxygen species [60] renders these kinetic investigations of physiopathological relevance. Thus, the role played by heme–HSA in the detoxification process is significantly enhanced by the fact that the amount of heme–HSA increases significantly under pathological conditions [9, 10, 61, 62] owing to the function of HSA as a heme scavenger from HDL and LDL, impairing their oxidation [8, 48, 49].

Furthermore, this behavior, which underlies the occurrence of multiple conformations of iron(II) heme–HSA, may have great impact on the function of heme–HSA as a metabolite and drug transporter, since this proton-linked modulation is reflected in its capability of interacting with molecules circulating in the bloodstream, as previously demonstrated [3, 8, 20, 22, 29–32]. Therefore, HSA, not only acting as a heme carrier but also displaying transient heme-based properties, represents a case for "chronosteric effects" [62], which opens the scenario toward the possibility of a time- and metabolite-dependent multiplicity of roles for HSA.

References

1. Kragh-Hansen U (1981) Pharmacol Rev 33:17–53
2. Carter DC, Ho JX (1994) Adv Protein Chem 45:153–203
3. Peters T Jr (1996) In all about albumin: biochemistry genetics and medical applications. Academic Press, San Diego
4. Monzani E, Bonafé B, Fallarini A, Redaelli C, Casella L, Minchiotti L, Galliano M (2001) Biochim Biophys Acta 1547:302–312
5. Curry S (2002) Vox Sang 83(Suppl. 1):315–319
6. Kragh-Hansen U, Chuang VT, Otagiri M (2002) Biol Pharm Bull 25:695–704
7. Sakurai Y, Ma SF, Watanabe H, Yamaotsu N, Hirono S, Kurono Y, Kragh-Hansen U, Otagiri M (2004) Pharm Res 21:285–292
8. Ascenzi P, Bocedi A, Visca P, Altruda F, Tolosano E, Beringhelli T, Fasano M (2005) IUBMB Life 57:749–759
9. Fasano M, Curry S, Terreno E, Galliano M, Fanali G, Narciso P, Notari S, Ascenzi P (2005) IUBMB Life 57:787–796
10. Ascenzi P, Bocedi A, Notari S, Fanali G, Fesce R, Fasano M (2006) Mini Rev Med Chem 6:483–489
11. Ascenzi P, Fasano M (2010) Biophys Chem 148:16–22
12. He X, Carter DC (1992) Nature 358:209–215
13. Sugio S, Kashima A, Mochizuki S, Noda M, Kobayashi K (1999) Protein Eng 12:439–446
14. Wardell M, Wang Z, Ho JX, Robert J, Rüker F, Ruble J, Carter DC (2002) Biochem Biophys Res Commun 291:813–819
15. Simard JR, Zunszain PA, Hamilton JA, Curry S (2006) J Mol Biol 361:336–351
16. Fasano M, Fanali G, Leboffe L, Ascenzi P (2007) IUBMB Life 59:436–440
17. Ascenzi P, Fasano M (2009) IUBMB Life 61:1118–1122
18. Sudlow G, Birkett DJ, Wade DN (1975) Mol Pharmacol 11:824–832
19. Diana FJ, Veronich K, Kapoor AL (1989) J Pharm Sci 78:195–199
20. Yamasaki K, Maruyama T, Yoshimoto K, Tsutsumi Y, Narazaki R, Fukuhara A, Kragh-Hansen U, Otagiri M (1999) Biochim Biophys Acta 1432:313–323
21. Dockal M, Chang M, Carter DC, Rüker F (2000) Protein Sci 9:1455–1465
22. Baroni S, Mattu M, Vannini A, Cipollone R, Aime S, Ascenzi P, Fasano M (2001) Eur J Biochem 268:6214–6220
23. Petitpas I, Bhattacharya AA, Twine S, East M, Curry S (2001) J Biol Chem 276:22804–22809
24. Ghuman J, Zunszain PA, Petitpas I, Bhattacharya AA, Otagiri M, Curry S (2005) J Mol Biol 353:38–52
25. Bhattacharya AA, Curry S, Franks NP (2000) J Biol Chem 275:38731–38738
26. Bhattacharya AA, Grüne T, Curry S (2000) J Mol Biol 303:721–732
27. Curry S (2009) Drug Metab Pharmacokinet 24:342–357
28. Simard JR, Zunszain PA, Ha CE, Yang JS, Bhagavan NV, Petitpas I, Curry S, Hamilton JA (2005) Proc Natl Acad Sci USA 102:17958–17963
29. Fasano M, Baroni S, Vannini A, Ascenzi P, Aime S (2001) J Biol Inorg Chem 6:650–658
30. Mattu M, Vannini A, Coletta M, Fasano M, Ascenzi P (2001) J Inorg Biochem 84:293–296
31. Fasano M, Mattu M, Coletta M, Ascenzi P (2002) J Inorg Biochem 91:487–490
32. Fanali G, De Sanctis G, Gioia M, Coletta M, Ascenzi P, Fasano M (2009) J Biol Inorg Chem 14:209–217
33. Zunszain PA, Ghuman J, Komatsu T, Tsuchida E, Curry S (2003) BMC Struct Biol 3:6
34. Nicoletti FP, Howes BD, Fittipaldi M, Fanali G, Fasano M, Ascenzi P, Smulevich G (2008) J Am Chem Soc 130:11677–11688
35. Dill K, Alonso DOV, Hutchinson K (1989) Biochemistry 28:5439–5449
36. Komatsu T, Matsukawa Y, Tsuchida E (2000) Bioconjug Chem 11:772–776
37. Kamal JK, Behere DV (2002) J Biol Inorg Chem 7:273–283
38. Komatsu T, Ohnichi N, Nakagawa A, Zunszain PA, Curry S, Tsuchida E (2005) J Am Chem Soc 127:15933–15942
39. Komatsu T, Nakagawa A, Curry S, Tsuchida E, Murata K, Nakamura N, Ohno H (2009) Org Biomol Chem 7:3836–3841
40. Monzani E, Curto M, Galliano M, Minchiotti L, Aime S, Baroni S, Fasano M, Amoresano A, Salzano AM, Pucci P, Casella L (2002) Biophys J 83:2248–2258
41. Fanali G, Fesce R, Agrati C, Ascenzi P, Fasano M (2005) FEBS J 272:4672–4683
42. Fanali G, Bocedi A, Ascenzi P, Fasano M (2007) FEBS J 274:4491–4502
43. Fanali G, Pariani G, Ascenzi P, Fasano M (2009) FEBS J 276:2241–2250
44. Bocedi A, Notari S, Menegatti E, Fanali G, Fasano M, Ascenzi P (2005) FEBS J 272:6287–6296
45. Tsuchida E, Sou K, Nakagawa A, Sakai H, Komatsu T, Kobayashi K (2009) Bioconjug Chem 20:1419–1440
46. Ascenzi P, Fasano M (2007) Biochem Biophys Res Commun 353:469–474

47. Ascenzi P, di Masi A, Coletta M, Ciaccio C, Fanali G, Nicoletti FP, Smulevich G, Fasano M (2009) J Biol Chem 284:31006–31017
48. Miller YI, Shaklai N (1999) Biochim Biophys Acta 1454:153–164
49. Tolosano E, Fagoonee S, Morello N, Vinchi F, Fiorito V (2010) Antioxid Redox Signal 12:305–320
50. Marden MC, Hazard ES, Leclerc L, Gibson QH (1989) Biochemistry 28:4422–4426
51. Kharitonov VG, Sharma VS, Magde D, Koesling D (1997) Biochemistry 36:6814–6818
52. Boffi A, Das TK, Della Longa S, Spagnuolo C, Rousseau DL (1999) Biophys J 77:1143–1149
53. Antonini E, Brunori M (1971) Hemoglobin and myoglobin in their reactions with ligands. North-Holland, Amsterdam
54. Razzera G, Vernal J, Baruh D, Serpa VI, Tavares C, Lara F, Souza EM, Pedrosa FO, Almeida FC, Terenzi H, Valente AP (2008) J Biol Inorg Chem 13:1085–1096
55. Ray GB, Li XY, Ibers JA, Sessler JL, Spiro TG (1994) J Am Chem Soc 116:162–176
56. Vogel KM, Kozlowski PM, Zgierski MZ, Spiro TG (2000) Inorg Chim Acta 297:11–17
57. Spiro TG, Wasbotten IH (2005) J Inorg Biochem 99:34–44
58. Ye X, Yu A, Georgiev GY, Gruia F, Ionascu D, Cao W, Sage JT, Champion PM (2005) J Am Chem Soc 127:5854–5861
59. Coletta M, Angeletti M, De Sanctis G, Cerroni L, Giardina B, Amiconi G, Ascenzi P (1996) Eur J Biochem 235:49–53
60. Piantadosi CA (2008) Free Radic Biol Med 45:562–569
61. Müller-Eberhard U, Javid J, Liern HH, Hanstein A, Hanna M (1968) Blood 32:811–815
62. Fasano M, Fanali G, Fesce R, Ascenzi P (2008) Human serum heme-albumin: an allosteric "chronosteric" protein. In: Bolognesi M, Di Prisco G, Verde C (Eds.) Dioxygen Binding and Sensing Proteins. Protein Reviews, Vol 9, pp 121–131. Springer, Heidelberg
63. Lukat-Rodgers GS, Rodgers KR, Caillet-Saguy C, Izadi-Pruneyre N, Lecroisey A (2008) Biochemistry 47:2087–2098
64. Liu Y, Moenne-Loccoz P, Hildebrand DP, Wilks A, Loehr TM, Mauk AG, Ortiz de Montellano PR (1999) Biochemistry 38:3733–3743
65. Sage J, Morikis D, Champion PM (1991) Biochemistry 30:1227–1237
66. Ling JH, Li TS, Olson JS, Bocian DF (1994) Biochim Biophys Acta 1188:417–421
67. Ramsden J, Spiro TG (1989) Biochemistry 28:3125–3128